ARTICLES
PUBLISHED ONLINE: 4 AUGUST 2013 | DOI: 10.1038/NMAT3722
nature materials

# A general relationship between disorder, aggregation and charge transport in conjugated polymers

Rodrigo Noriega[1†‡], Jonathan Rivnay[2†‡], Koen Vandewal[2], Felix P. V. Koch[3], Natalie Stingelin[3,4], Paul Smith[3], Michael F. Toney[5] and Alberto Salleo[2*]

**Conjugated polymer chains have many degrees of conformational freedom and interact weakly with each other, resulting in complex microstructures in the solid state. Understanding charge transport in such systems, which have amorphous and ordered phases exhibiting varying degrees of order, has proved difficult owing to the contribution of electronic processes at various length scales. The growing technological appeal of these semiconductors makes such fundamental knowledge extremely important for materials and process design. We propose a unified model of how charge carriers travel in conjugated polymer films. We show that in high-molecular-weight semiconducting polymers the limiting charge transport step is trapping caused by lattice disorder, and that short-range intermolecular aggregation is sufficient for efficient long-range charge transport. This generalization explains the seemingly contradicting high performance of recently reported, poorly ordered polymers and suggests molecular design strategies to further improve the performance of future generations of organic electronic materials.**

Systematic progress in materials engineering is best guided by a fundamental understanding of the impact of structure—from atomic to microstructural and mesoscopic scales—on functional properties. Structural control at the appropriate length scales combined with knowledge of basic physical processes have given rise to engineering breakthroughs and rational design of new materials. For instance, the understanding of how chain alignment and degree of crystallinity control the mechanical properties of polymers led to the development of fibres with specific strengths exceeding that of steel. Recently, the potential to combine low-cost manufacturing and mechanical robustness while simultaneously engineering optoelectronic properties has spurred great interest in semiconducting polymers[1]. Consequently, devices based on organic semiconductors have reached significant milestones, such as ~10% solar power conversion efficiencies[2] and electron and hole mobilities exceeding 1 $cm^2\ V^{-1}\ s^{-1}$ (refs 3,4). In contrast with other semiconductors, there is no commonly accepted, widely applicable model of charge transport in semiconducting polymers. Depending on the materials, models used to describe charge transport in organic semiconductors include band transport, hopping or multiple trapping and release[1]. Except for dynamic localization[5], most of these models have been adapted from the study of inorganic semiconductors, where atoms are strongly localized on their equilibrium lattice sites. In contrast, conjugated polymers are weakly bonded macromolecules with numerous degrees of conformational freedom, resulting in microstructures varying from completely amorphous to crystalline. Typical crystalline packing in semicrystalline conjugated polymers involves ordered lamellae composed of co-facially stacked molecules that exhibit strong $\pi$-orbital overlap (Supplementary Fig. S1).

Based on the observation that inorganic polycrystalline semiconductors often transport charge better than their amorphous analogues, much of the progress in the design of semiconducting polymers was made by pursuing polycrystalline-like microstructures. However, recent polymers based on increasingly complex monomers[3,6–13] seem to refute old paradigms exploited to attain high mobility, such as those involving regioregularity, texture, or crystallinity[10,14–16]. More significantly, highly disordered or even seemingly amorphous polymers now perform as well as semicrystalline materials[4,10].

The interplay between microstructure and electrical properties in conjugated polymers is far from being clearly articulated. This difficulty originates from these materials' intermediate location on the order–disorder scale. Materials that are between (poly)crystalline and amorphous are, in general, poorly understood. In this manuscript, we place in a common context both new data and literature data by applying characterization principles that allow a ranking of conjugated polymers according to their degree of structural disorder. All materials for which there exist relevant data, when processed into their highest-performing microstructure, exhibit a large amount of lattice disorder irrespective of their chemistry or overall degree of crystallinity. Structural disorder is linked to electronic localization within molecular stacks and gives rise to electronic traps, which limit charge transport in high-mobility conjugated polymers. This powerful simplification reveals a general structure–property

[1]Department of Applied Physics, Stanford University, Stanford, California 94305, USA, [2]Department of Materials Science and Engineering, Stanford, California 94305, USA, [3]Department of Materials, ETH Zurich, Zurich 8093, Switzerland, [4]Department of Materials and Centre of Plastic Electronics, Imperial College London, London SW7 2AZ, UK, [5]Stanford Synchrotron Radiation Lightsource (SSRL), SLAC National Accelerator Laboratory, Menlo Park, California 94025, USA. †These authors contributed equally to this work. ‡Present addresses: Department of Chemistry, University of California Berkeley, 94720, USA (R.N.); Department of Bioelectronics, Ecole Nationale Supérieure des Mines, CMP-EMSE, MOC, 13541 Gardanne, France (J.R.).
*e-mail: asalleo@stanford.edu

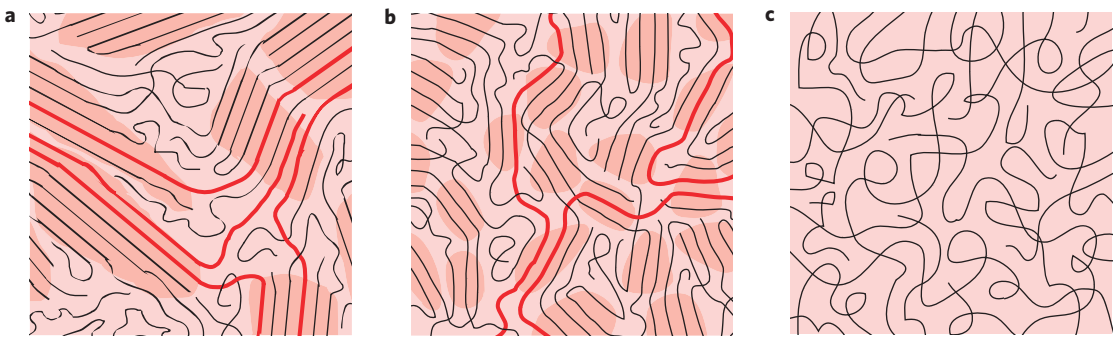


**Figure 1 | Microstructure of conjugated polymer films. a–c**, Schematics of the microstructure of a semicrystalline polymer film, for example P3HT (**a**), disordered aggregates (**b**) and a completely amorphous film (**c**). Note the coexistence of ordered (darker shadowed areas) and spaghetti-like amorphous regions. This microstructure is similar to the concept of fringed micelles. If the molecular weight is high enough and there is a large enough density of ordered material, long polymer chains (highlighted in red) can connect ordered regions without a significant loss of conjugation, greatly improving charge transport.

relationship relating order at the segmental level to transport at the device scale. A survey of over ten years of literature data confirms the generality of these concepts.

## Charge transport and the importance of aggregates

The microstructure of high-molecular-weight poly(3-hexylthiophene), P3HT—a model semicrystalline conjugated polymer—exhibits a continuous variation in order parameters[17,18] where semi-ordered and amorphous 'spaghetti-like' regions coexist; long polymer chains are responsible for the connectivity between adjacent crystallites (Fig. 1a)[19]. Semi-ordered regions may be comprised of large domains with three-dimensional long-range periodicity (crystallites) or smaller domains with short-range ordering of a few molecular units (aggregates, which may also be identified as fringed micelles; Fig. 1b).

In such a heterogeneous microstructure, the ordered regions are largely responsible for charge transport because charges must overcome an energy barrier to move from ordered to amorphous regions. Indeed, owing to its reduced conjugation length, the amorphous fraction of regio-regular P3HT (RR-P3HT) has a larger bandgap compared to the aggregates and we find no evidence of energetic overlap of electronic states in amorphous and ordered P3HT regions (Supplementary Fig. S2). This energetic offset hinders carrier migration into the amorphous regions, and makes it energetically and statistically favourable for charges at the order/disorder interface to migrate back into the ordered regions. Because, in principle, this offset could be reduced by polaronic effects, we test our hypothesis by studying blends of regio-random P3HT (RRa-P3HT) with controlled amounts of RR-P3HT nanofibrils (see Methods)[20]. Even for a low concentration of aggregates (~10% by volume), at current densities comparable to those encountered in electronic devices, the electroluminescence spectra resemble that of RR-P3HT (Fig. 2, and Supplementary Figs S3 and S4). Consequently, transported charges recombine within fibrils. Thus, at realistic current densities, charge carriers remain confined in the ordered regions of a heterogeneous microstructure when such ordered regions are spatially close enough to form an interconnected network through tie-molecules.

This conclusion may be challenged by the oft-encountered assumption, based on calorimetric measurements, that semicrystalline polymer films have a low degree of crystallinity. However, these measurements systematically underestimate the amount of ordered material (Supplementary Fig. S5). In P3HT, we assess that such an underestimation is approximately a factor of two, with the aggregate volume fraction in P3HT films near ~40–50% (refs 21,22). Hence, in high-mobility polymers the fraction of the film comprised of ordered material is sufficiently large to be interconnected by bridging polymer chains, creating a network that sustains efficient charge transport. Such networks of crystallites have been previously observed in conjugated polymers[21,23].

The nature of the connections between aggregates is poorly understood and should be the subject of further study. Nevertheless, we are able to make a few qualitative considerations. Polymer chains are semiflexible[24,25]—that is, rigid at length scales comparable to their persistence length and flexible at larger length scales. If the spacing between neighbouring crystallites is only a few persistence lengths, a chain that exits one ordered region and enters

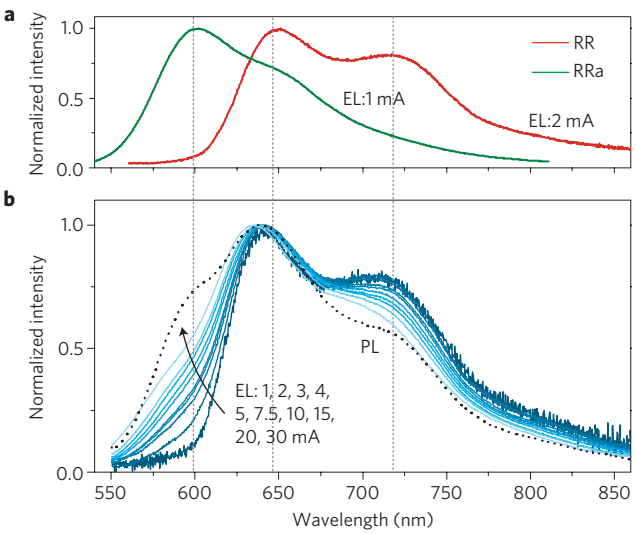


**Figure 2 | Photo-physical characterization of pre-aggregated P3HT fibril:amorphous-blend films. a**, Reference electroluminescence spectra from pure RR and RRa P3HT. Vertical dashed lines are the electroluminescence peak positions for the amorphous, and 0-0, 0-1 aggregate transitions of the pristine films, respectively. **b**, Photoluminescence spectrum (dotted) showing the signature of aggregated and amorphous material, along with electroluminescence spectra for increasing values of current in the devices made with films of 10% pre-aggregated RR-P3HT. Unlike the photoluminescence spectrum, the low-current (typical of normal device application) electroluminescence spectra show only emission from aggregates, indicating that it is due exclusively to recombination within the aggregates and not to exciton energy transfer to the aggregates before recombination. Only at large current densities does the blue-shifted spectral feature from RRa-P3HT appear, indicating emission from the disordered matrix.

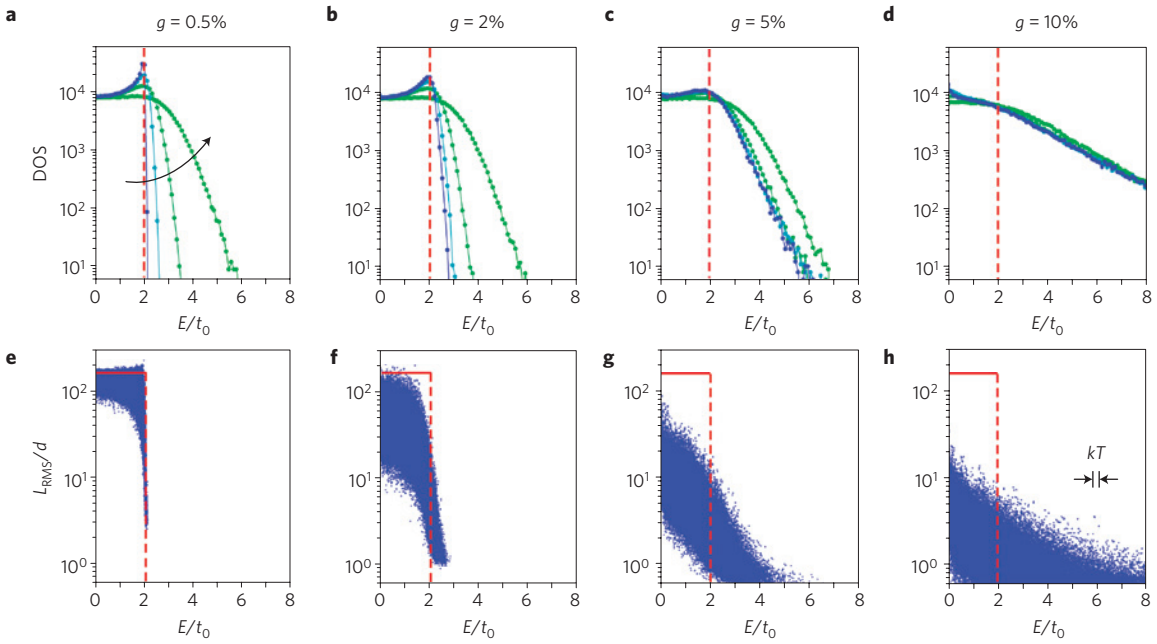


**Figure 3 | Modelling of the electronic effects of energetic and structural disorder. a–d**, DOS of 1D stacks with different amounts of lattice disorder ($g$) and Gaussian energetic disorder (of width $\sigma$). We show the cases of an almost perfect lattice ($g = 0.5\%$; **a**), a lattice with a small amount of disorder ($g = 2\%$; **b**), a moderately paracrystalline lattice ($g = 5\%$; **c**), and a strongly disordered lattice ($g = 10\%$; **d**). The widths of the probability distribution of on-site energies increase as indicated by the arrow in **a** in the sequence 0, 50, 100 and 200 meV. The energy coordinate is normalized by the inter-site transfer integral at equilibrium, $t_0 = 150$ meV. **e–h**, Localization length (that is, the root mean square spatial extent) for each of the eigenstates of the disordered Hamiltonian, normalized by the inter-site distance $d$, plotted versus the state's energy. No energetic disorder was included, and the amounts of paracrystalline disorder are the same as **a–d**. The box depicts the localization length of states in a perfect stack (red horizontal line: complete delocalization) and the band edge in the absence of disorder (dashed line). States with a normalized localization length $<2$ are considered completely localized. The magnitude of $kT$ at room temperature is indicated in **h**.

another should not suffer large bends in its backbone and should retain significant conjugation. Such a chain segment, although not part of any aggregate, provides an efficient charge transport pathway between ordered regions and acts as a tie-molecule (see Supplementary Text). Hence, in high-molecular-weight polymers, transport occurs through an interconnected network of ordered regions. The amorphous fraction of the film does not participate in transport; therefore, the structural properties of the ordered regions govern charge transport in the film. Local mobility measurements in high-molecular-weight P3HT confirm that mobility is limited by transport in these nanoscale aggregates[26], and scanning-probe field-effect measurements show no barrier for charge transport between aggregates[27]. These and our findings demonstrate experimentally that the electrical connection between aggregates is not a rate-limiting step in the transport process for conjugated polymers of sufficiently high molecular weight.

## Effect of disorder on the electronic structure of aggregates

As charges in semicrystalline polymers reside in the ordered regions of the film, the effect of structural imperfections in these regions on their electronic properties must be understood. Structural disorder gives rise to energetic disorder—that is, variations in the energy levels across the material—and also affects intermolecular charge transfer integrals. Disorder-induced localization is a well-known occurrence in condensed matter[28,29]. Semiconducting polymers, however, require the understanding of charge transport in intermediate disorder regimes. Structural disorder in an imperfect crystal is described by the paracrystallinity model as random fluctuations in lattice spacings. This disorder is quantitatively measured by the paracrystallinity parameter $g$, which is the standard deviation of local static lattice fluctuations normalized by the average value of the lattice spacing[30]. Interestingly, paracrystallinity describes the local structure of amorphous silicon more accurately than previously accepted models[31].

The strongest electronic coupling in a polymer is along its backbone, but intermolecular transport is necessary in a typical device as no individual chain can provide macroscopic transport. Disorder in the π-stacks of organic semiconductors is most relevant to transport because this direction supports rate-limiting intermolecular charge transfers. Paracrystallinity in the π-stacks causes the creation of deep tails of electronic states extending into the materials' bandgap with a characteristic energy breadth proportional to $g^2$ (ref. 32). To compare the effects of structural and energetic disorder on electronic structure, we use a tight-binding model where an aggregate is modelled as a 1D π-stack of molecules (Methods and Supplementary Text). Including variations in the molecular energy levels as well as fluctuations in the intermolecular charge transfer integral yields results useful for qualitative comparisons.

In the case of negligible paracrystallinity, the density of states (DOS) of the 1D π-stack depends on the amount of on-site disorder generating a Gaussian tail of states extending into the bandgap (Fig. 3a). Typical π-stacks of conjugated polymers exhibit moderate amounts of paracrystalline disorder ($g \geq 5\%$; see below). Under these conditions, the DOS of the aggregate is hardly affected by on-site disorder and is determined by the amount of paracrystallinity (Fig. 3c,d).

Our model neglects dynamic effects, which were included in a recent study[33] of charge transport in poly(2,5-bis(3-tetradecylthiophen-2-yl)thieno[3,2,-b]thiophene) (PBTTT), where the authors suggested that dynamic fluctuations and polarization-induced charge stabilization lead to further DOS broadening. Fluctuations of electronic couplings, however, occur on a very fast timescale and must be time-averaged before studying charge transfer events. Although our treatment includes no time

dependence, static cumulative disorder is significant in these materials. Dynamic disorder will induce further fluctuations around the static positions, but these refinements do not qualitatively alter our conclusions.

The spatial extent of the calculated wavefunctions for the disordered stack (Fig. 3e–h) shows that disorder-induced states that lie deeper into the DOS tail are increasingly localized. Even states within the originally 'delocalized band' become more localized with increasing paracrystallinity. In the limit of large positional disorder ($g \sim 10\%$), the distinction between band and tail disappears: a single broad distribution of localized states with a monotonically decreasing DOS extends into the bandgap, reproducing well-known results of electronic structure theory of amorphous materials[34,35]. In the intermediate paracrystallinity regime ($g \sim 3$–$7\%$) we observe a coexistence of localized and delocalized states, indicating that in paracrystalline aggregates charge is transported by a mechanism where mobile charge is temporarily trapped in localized states, akin to multiple trapping and release[1,36].

## Measuring paracrystallinity in conjugated polymers

Using X-ray diffraction peak-shape analysis (details in Supplementary Text) we quantify paracrystallinity in polymer crystallites to determine whether this disorder dominates their DOS. In PBTTT, a polymer considered to exhibit an exceptional degree of order[37], we find a highly anisotropic lattice disorder. In the lamellar stacking direction, $g_{lam} = 2.6\%$ owing to side chain interdigitation[38,39]. Long-range lamellar order however does not translate to order in the π-stacks, where $g_{\pi} = 7.3\%$, a value close to that of an amorphous stack. Thus, we conclude that the DOS of a PBTTT π-stack is dictated by paracrystalline disorder.

The low amount of paracrystalline disorder measured in a small molecule film and its small anisotropy (Fig. 4 and Supplementary Table S1) shows that organic solids are not inherently disordered in spite of their weak intermolecular forces. Conversely, the distinguishing feature of polymers is the pronounced disorder in the π-stacking direction. To observe this transition, we use thin films of P3HT with chain lengths of 8 to >2,000 monomers ($M_n$ from 1.33 to >350 kg mol$^{-1}$), and perform single-peak estimations of the π-stacking disorder (Supplementary Text and Figs S6, S7). When starting from an oligomer and adding monomers to form a high-molecular-weight polymer, paracrystallinity in the π-stacking direction is initially low (comparable to that in polycrystalline films of small molecules) and rises until the incremental effect of adding monomers vanishes and paracrystallinity becomes independent of molecule length (Fig. 4a).

Although P3HT represents a model system, we also explored paracrystallinity in the π-stacking direction of other high-mobility polymers. We collect π-stacking data from over 30 literature cases (Fig. 4a), where conjugated polymers were processed with common solvents and casting techniques. It is apparent that high-molecular-weight semicrystalline polymer semiconductors exhibit a surprisingly common level of minimum lattice disorder ($g \sim 6$–$8\%$). In the direction where intermolecular charge transfer occurs, all high-mobility high-molecular-weight polymers are closer to being amorphous ($g \sim 10$–$20\%$) than crystalline ($g < 1\%$), irrespective of the degree of order in the lamellar stacking direction. The universal dependence of paracrystalline disorder on molecular weight indicates that chain folding and entanglements are probable sources of defects[40]. Side-chain conformational disorder may also disrupt the backbone packing arrangement, leading to an intrinsic level of disorder common to all conjugated polymers.

A simultaneous comparison of the effect of molecular weight on disorder and on mobility (Fig. 4) is a strong indication that charge transport is linked to lattice disorder. When the molecular weight of P3HT is high enough such that its lattice disorder becomes independent of chain length, the carrier mobility is also

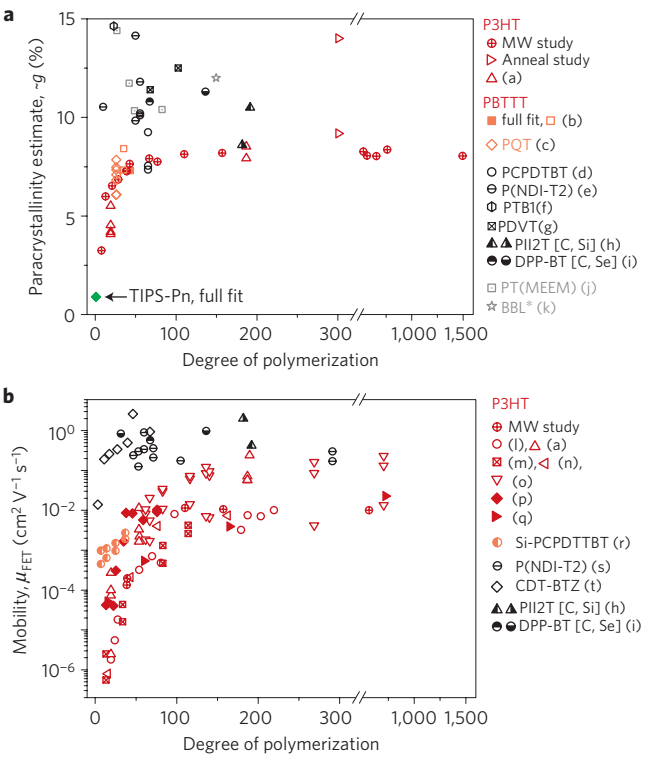


**Figure 4 | Chain length effects on paracrystallinity and charge transport.** **a**, The π-stacking paracrystallinity in films of polymeric semiconductors of different molecular weight (MW), plotted as a function of degree of polymerization. Semicrystalline materials (P3HT, PBTTT, PQT) are shown in shades of red. Poorly ordered high performing materials are shown in black. Others are shown in grey. Open symbols are estimates, solid symbols are derived from a full analysis. As a comparison, cumulative disorder in polycrystalline triisopropylsilyl pentacene (TIPS-Pn) is far smaller than that of PBTTT and, importantly, shows significantly less anisotropy (Supplementary Table S1). **b**, Mobility as a function of molecular weight for a variety of semiconducting polymers. P3HT is shown in red with different symbols referring to different studies. Other high-performing materials are shown in black. For the complete list of references see Supplementary Text.

remarkably independent of chain length. The link between these two fundamentally different properties is particularly striking, as the turn-over point is the same for both (chains with 50–100 monomers for P3HT) and agrees with recent yield and mobility measurements of photogenerated charges[41]. Our findings remain valid, irrespective of whether interface or bulk measurements are considered (see Supplementary Text). Similar improvements in mobility with increasing molecular weight have been observed in other polymers[11,42].

The effect of molecular weight on charge transport in semicrystalline polymers is subject to an intrinsic and general trade-off. Long chains provide electrical connectivity between ordered regions, allowing efficient charge transport, but also result in higher structural disorder. In the low-molecular-weight connectivity-limited regime, mobility rises quickly as average chain length increases[43]. Eventually, the mobility plateaus as a function of molecular weight when enough connectivity is provided for charge to move through the paracrystalline regions (see Supplementary Text). Thus, in high-molecular-weight polymers charge transport is strongly enhanced by the connectivity of the ordered regions (crystallites and aggregates) but limited by lattice disorder in these regions once sufficient connectivity is established.

The spread in mobility values is significant, showing that no single microstructural feature is entirely responsible for electronic

performance. Differences in morphology arise from variations in processing conditions and polydispersity, which contribute to the variability in charge carrier mobility. Despite these factors, the fundamental transport-limiting mechanism and its causal connection to paracrystallinity is preserved.

## Paracrystallinity governs charge transport

In 'classic' (that is, designed to exhibit a noticeable degree of crystallinity and extended π–π stacking) semicrystalline conjugated polymers, paracrystalline disorder in the crystallites limits charge transport via the introduction of traps. The level of lattice disorder in the π-stacking direction measured in all high-molecular-weight polymers corresponds to the regime where localized and delocalized states in the aggregates coexist, giving rise to trapping-limited transport, as experimentally observed in field effect transistors (FET) and in local mobility measurements[26]. In FETs, the difference in energy between the populated traps and the mobile states manifests itself in the activation energy for transport and its dependence on charge density (gate voltage). Hence, the greater the disorder, the deeper the traps and the larger the activation energy.

In Fig. 5, we gather activation energies derived from temperature-dependent FET measurements, and trap depth/tail widths derived from modelling electrical transport both from the literature and from this work. These data were collected from samples spanning a range of mobility, materials purity, device preparation, surface treatments and geometry. In spite of such variety of materials and conditions, a consistent behaviour emerges. Transport in common thiophene-based semicrystalline polymers—for example, P3HT, poly[5,5′-bis(3-alkyl-2-thienyl)-2,2′-bithiophene] (PQT), PBTTT—has an average $72 \pm 24$ meV activation energy. In comparison, completely amorphous materials show a significantly higher average activation energy $\sim 230 \pm 100$ meV. It is interesting to examine new high-performance polymers, which do not seem to belong in either category. Examples of these materials are copolymers based on more complex moieties, such as naphthalene-diimides (PNDI-T2), diketopyrrolopyrroles with sulphur and selenium (DPP-BT, DSePP-BT), and carbazoles (PCDTBT), but also newer materials such as isoindigo copolymers and indacenodithiophene-based polymers. These materials have mobilities comparable to those of semicrystalline polymers ($\mu_{FET} \sim 1\ cm^2\ V^{-1}\ s^{-1}$), but at first glance, morphologically, they are closer to the amorphous materials family. Indeed their disorder is higher than that of semicrystalline polymers, as evidenced by lower diffracted intensities, fewer observable diffraction peaks, and/or the large breadth of their π-stacking peak. These new high-mobility polymers exhibit activation energies and trap breadths of $76 \pm 33$ meV: similar to those of 'classic' semicrystalline polymers and significantly lower than the mean value observed for amorphous conjugated polymers. Many of these new reportedly 'amorphous' materials have at least enough short-range order to result in detectable diffraction in synchrotron XRD experiments (Supplementary Fig. S8). Though polymers in this new class are seemingly disordered, they exhibit the tell-tale signs of aggregation in their solid-state optical absorption spectra, namely the presence of a resolvable vibronic progression near the absorption edge[22]. Short-range order in the form of aggregates is sufficient to support efficient intermolecular charge transfer. Because charges have a short scattering mean free path in the π-stacks—on the order of a nanometre[36]—they are mostly affected by such short-range order. Disordered crystallites larger than a scattering length bring hardly any additional benefit for charge transport. In conjugated polymers, crystallinity—no matter how low—is a sign that the polymer chains have a tendency to form stacked aggregates with a paracrystallinity that can be estimated by the width of the π-stacking XRD peak. This collection of interconnected aggregates enables high mobilities in high-molecular-weight polymers despite the consistently large

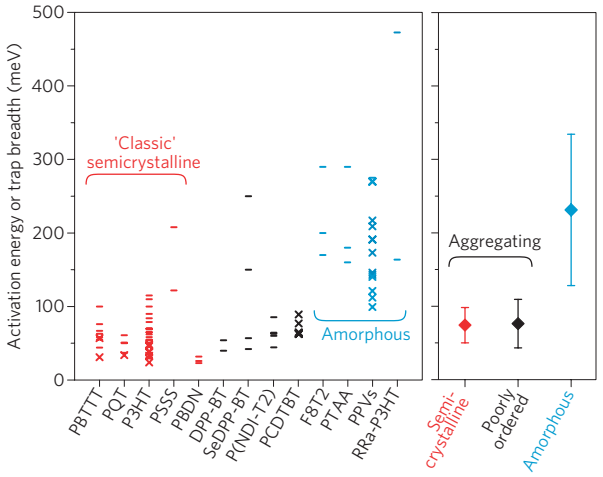


**Figure 5 | Activation energy for transport in semiconducting polymers.** Activation energies obtained from FET data from this work, and from the literature (dash), as well as trap depth/tail widths derived from device modelling (cross) for traditional classic semicrystalline materials (red), new high performers that are found to be poorly ordered (black), and completely amorphous materials (blue). Data (84 values for 13 different materials) are binned by material (for the complete list of references see Supplementary Text). The averages and standard deviations from the respective groups are shown for semicrystalline, poorly ordered, and amorphous materials on the right panel.

paracrystalline disorder in the π-stacking direction and weak diffracted intensities.

Molecular stacking, even with only short-range order, makes aggregating materials fundamentally different from truly amorphous polymers. Assuming an exponential dependence of the intermolecular transfer integral $t$ on separation $x$, $t = t_0 e^{-\beta x}$, the prefactor $t_0$ and wavefunction overlap decay length $(1/\beta)$ govern the extent to which lattice disorder affects charge transport. The newer high-mobility polymers can tolerate nanometre-scale disorder owing to their structure at the ångström-scale. For example, increasing $t_0$ by reducing the π–π stacking distance causes aggregates to be electronically less sensitive to large amounts of disorder, increasing the threshold beyond which paracrystallinity-induced states severely affect transport. Similarly, reducing $\beta$ by designing materials with orbitals having larger overlaps or favourable symmetries reduces the effect of positional disorder on charge transport. Some of these factors are probably at work in recently reported high-mobility polymers. The optimization of side-chains to increase solubility leads to a reduced intermolecular π-stacking distance in diketopyrrolopyrrole-furan and isoindigo-based polymers. Using large and planar fused-ring aromatic cores increases the overlapping area between adjacent π-stacked units, making the aggregates less sensitive to positional disorder[12,13]. Therefore, tuning the molecular design to improve packing and orbital shape, orientation and symmetry may contribute to making transport in aggregates—where charge is confined—less sensitive to π-stacking disorder, thereby preserving efficient device-scale charge transport.

These considerations separate polymeric semiconductors into two classes. In one class we have truly amorphous materials, lacking any long-range order and characterized by broad, featureless amorphous X-ray scattering halos. Charge transport in these truly amorphous materials is limited by hopping between localized states in a broad DOS. Such a transport mode is restricted to mobilities $<0.1\ cm^2\ V^{-1}\ s^{-1}$ and is subject to large activation energies[44]. In the second class are materials that can form interconnected aggregates exhibiting at least short-range order, with transport in field-effect devices described by a multiple trapping and release mechanism.

The difference between aggregating materials families is the distance over which aggregation persists: semi-crystalline materials exhibit relatively long range order (several to 10 s of nanometres in the π-stacking direction as derived from the coherence length) and strong X-ray scattering, whereas weakly scattering polymers can be ordered in some crystallographic directions (alkyl-stacking) but remain largely disordered in the π-stacking direction (Supplementary Fig. S8). Even though these semi-amorphous materials are strongly disordered in their π-stacks, their ability to form aggregates allows locally efficient intermolecular charge transport. Such short-range order at the segmental level is sufficiently pervasive in the thin-film microstructures to provide effective pathways for charge transport. Aggregating polymers of high molecular weight, whether very weakly diffracting or truly semicrystalline, belong to the same class, where the disorder in the intermolecular π-stacking direction is consistently high in all conjugated polymers and induces traps in the DOS, which are transport-limiting.

## Implications for high-mobility semiconducting polymers

Understanding charge transport in conjugated semicrystalline polymers has proved to be a challenging problem owing to the unusual range of disorder they exhibit. These materials are not well-ordered, yet they are not amorphous either. By bringing together data from years of research in conjunction with new insights, we formulate a link between the molecular- and micro-structure of high-mobility semiconducting polymers and their macroscopic electrical properties. These insights uncover strong similarities within seemingly diverse families of conjugated polymers and allow us to formulate a unified transport model. We find that, in the π-stacking direction, the lowest observed amount of lattice disorder in all high-performance—and necessarily high molecular weight—polymers is unexpectedly large and remarkably independent of material. The unifying requirement for high carrier mobility is the presence of interconnected aggregates, even if they are small and disordered. The key to designing high-mobility polymers is not in increasing crystallinity but rather in increasing their tolerance to an inevitably large amount of disorder within the aggregates by allowing more efficient intra- and intermolecular charge transport/transfer at the segmental level. The fundamental relationship presented here between short-range order in π-aggregates, aggregate connectivity, and macroscopic charge transport provides input for the design of new optoelectronic polymers with the potential to usher in technological successes comparable to those obtained with high-strength polymers. More broadly, we provide a general framework for understanding how to take advantage of intermediate order at different length scales to control the macroscopic properties of semicrystalline polymers, be they optical, electrical or mechanical.

## Methods

**Sample preparation.** Samples for structural determination and TFT measurements were prepared on native oxide silicon and 200 nm thermal oxide silicon, respectively. Substrates were sonicated in acetone and isopropyl alcohol before drying with nitrogen and undergoing ultraviolet ozone treatment (20 min). Raw materials were used as received from Merck Chemicals (TIPS-Pn, P3HT), Polyera (N2200, and derivatives), Imperial College London (P3HT, PBTTT), and ETH Zurich (P3HT, P3HT-oligomers). Films were spin cast from ~10 mg ml$^{-1}$ solutions at 1,000–1,500; if used for electro-optical testing film formation was performed in a $N_2$ glove box (<1 ppm $O_2$). The samples in the P3HT molecular weight series were cast from toluene, whereas other films (TIPS-Pn, P3HT, P[NDI2OD-T2], PBTTT) were cast from dichlorobenzene. Directional samples of PBTTT were cast as previously described[45].

**Photo-physical characterization.** For electroluminescence (EL) and photoluminescence (PL) studies, we prepared solution blends of RRa-P3HT ($M_w$ = 90 kDa, $M_n$ = 30 kDa) and pre-aggregated RR-P3HT (regio-regularity ~97%, $M_w$ = 105 kDa, $M_n$ = 60 kDa). Starting solutions of RR- and RRa-P3HT in dichlorobenzene (DCB, 30 mg ml$^{-1}$) were dissolved at 80 °C overnight. To vary the amount of aggregated material in the films, the starting solutions of RR- and RRa-P3HT in DCB were diluted with ethylacetate (2:1 DCB:EtOAc solvent ratio) to form the stock solutions for pre-aggregated and amorphous materials, which were then mixed in 1:1 and 1:9 ratios. Films made from these solutions were spun cast onto ITO/PEDOT substrates and Ca/Al electrodes were evaporated to form devices with an area of 0.1 cm$^2$. The EL and PL spectra for these devices were collected using a cooled CCD camera and corrected for the spectrometer response. PL experiments used a pump beam from a 535 nm diode laser. The driving voltage for the diodes used in the EL measurements was provided by a Keithley 2400 power source. All these measurements and sample preparation were performed in an inert atmosphere.

**Electrical characterization.** For devices used for electrical characterization, substrates were first treated with an octadecyltrichlorosilane (OTS) self-assembled monolayer before casting of semiconducting polymer. The top 100 nm Au source and drain contacts were evaporated on dry films. Thin-film transistor devices were characterized in a vacuum probe station evacuated to $10^{-4}$ mbar. The TFT charge carrier mobility was extracted in the saturation regime ($V_d = -60$ V).

**X-ray characterization.** X-ray scattering was performed at the Stanford Synchrotron Radiation Lightsource (SSRL) on beamlines 7-2 (high-resolution grazing incidence), 2-1 (high-resolution specular), and 11-3 (2D scattering with an area detector, MAR345 image plate, at grazing incidence). The incident energy was 8 keV for beamlines 7-2 and 2-1, and 12.7 keV for beamline 11-3. The diffracted beam was collimated with 1 milliradian Soller slits for high-resolution in-plane scattering and with two 1 mm slits for specular diffraction. For both grazing incidence experiments, the incidence angle was slightly larger than the critical angle, ensuring that we sampled the full film depth. All X-ray measurements were performed in a helium-filled chamber to minimize beam damage and reduce air scattering. Data are expressed as a function of the scattering vector $q = 4\pi * \sin(\theta)/\lambda$, where $\theta$ is half the scattering angle and $\lambda$ is the wavelength of the incident radiation. Here, $q_{xy}$ ($q_z$) is the component of the scattering vector parallel (perpendicular) to the substrate. Only high-resolution measurements were employed for extraction of peak parameters and analysis of paracrystalline disorder. Details of the peak shape analysis, and resulting estimates and their justification can be found in the Supplementary Information and in ref. 46.

**Simulations.** The model from ref. 32 is simplified to a one-dimensional disordered stack made up of $N_s$ sites. A tight-binding Hamiltonian is employed to describe transport through this system, with on-site energies $\varepsilon_i$ and nearest neighbour transfer integrals $t_i$. In the matrix form of the Hamiltonian, the main diagonal reflects the on-site energies and the off-diagonal terms reflect inter-site couplings. To first order, we treat the observed fluctuation in lattice parameter within the crystalline regions only as a distribution of intermolecular separations, neglecting details of molecular orientation and correlations. Energetic disorder was introduced by selecting the on-site energies from a probability distribution of a given width; structural disorder is modelled by varying the coupling between neighbours as $t_i = t_0 e^{-\beta x_i}$, where the bond fluctuations $x_i$ due to lattice disorder modify the transfer integral at equilibrium $t_0$ with an exponential decay with characteristic length $1/\beta$. The transfer integral was parametrized according to values previously obtained for PBTTT (ref. 32). Solving for the eigenfunctions and eigenvalues of the Hamiltonian yields the states of the system and their energies, respectively.

Received 18 January 2013; accepted 25 June 2013; published online 4 August 2013

## References


1. Klauk, H. *Organic Electronics II: More Materials and Applications* (Wiley-VCH, 2012).
2. He, Z. *et al.* Enhanced power-conversion efficiency in polymer solar cells using an inverted device structure. *Nature Photon.* **6,** 593–597 (2012).
3. Chen, H. *et al.* Highly π-extended copolymers with diketopyrrolopyrrole moieties for high-performance field-effect transistors. *Adv. Mater.* **24,** 4618–4622 (2012).
4. Facchetti, A. π-conjugated polymers for organic electronics and photovoltaic cell applications. *Chem. Mater.* **23,** 733–758 (2010).
5. McMahon, D. P. & Troisi, A. Organic semiconductors: Impact of disorder at different timescales. *ChemPhysChem* **11,** 2067–2074 (2010).
6. Chen, Z. *et al.* High-performance ambipolar diketopyrrolopyrrole-thieno[3,2-b]thiophene copolymer field-effect transistors with balanced hole and electron mobilities. *Adv. Mater.* **24,** 647–652 (2012).
7. Jung, J. W., Liu, F., Russell, T. P. & Jo, W. H. A high mobility conjugated polymer based on dithienothiophene and diketopyrrolopyrrole for organic photovoltaics. *Energy Environ. Sci.* **5,** 6857–6861 (2012).
8. Kronemeijer, A. J. *et al.* A selenophene-based low-bandgap donor–acceptor polymer leading to fast ambipolar logic. *Adv. Mater.* **24,** 1558–1565 (2012).

9. McCulloch, I. *et al.* Design of semiconducting indacenodithiophene polymers for high performance transistors and solar cells. *Acc. Chem. Res.* **45,** 714–722 (2012).
10. Zhang, W. *et al.* Indacenodithiophene semiconducting polymers for high-performance, air-stable transistors. *J. Am. Chem. Soc.* **132,** 11437–11439 (2010).
11. Tsao, H. N. *et al.* Ultrahigh mobility in polymer field-effect transistors by design. *J. Am. Chem. Soc.* **133,** 2605–2612 (2012).
12. Mei, J., Kim, D. H., Ayzner, A. L., Toney, M. F. & Bao, Z. Siloxane-terminated solubilizing side chains: Bringing conjugated polymer backbones closer and boosting hole mobilities in thin-film transistors. *J. Am. Chem. Soc.* **133,** 20130–20133 (2011).
13. Yiu, A. T. *et al.* Side-chain tunability of furan-containing low-band-gap polymers provides control of structural order in efficient solar cells. *J. Am. Chem. Soc.* **134,** 2180–2185 (2012).
14. Sirringhaus, H. *et al.* Two-dimensional charge transport in self-organized, high-mobility conjugated polymers. *Nature* **401,** 685–688 (1999).
15. McMahon, D. P. *et al.* Relation between microstructure and charge transport in polymers of different regioregularity. *J. Phys. Chem. C* **115,** 19386–19393 (2011).
16. Rivnay, J. *et al.* Unconventional face-on texture and exceptional in-plane order of a high mobility n-type polymer. *Adv. Mater.* **22,** 4359–4363 (2010).
17. Watts, B., Schuettfort, T. & McNeill, C. R. Mapping of domain orientation and molecular order in polycrystalline semiconducting polymer films with soft x-ray microscopy. *Adv. Funct. Mater.* **21,** 1122–1131 (2011).
18. Collins, B. A. *et al.* Polarized X-ray scattering reveals non-crystalline orientational ordering in organic films. *Nature Mater.* **11,** 536–543 (2012).
19. Grevin, B., Rannou, P., Renaud, P., Pron, A. & Travers, J-P. Scanning tunneling microscopy investigations of self-organized poly(3-hexylthiophene) two-dimensional polycrystals. *Adv. Mater.* **15,** 881–884 (2003).
20. Scharsich, C. *et al.* Control of aggregate formation in poly(3-hexylthiophene) by solvent, molecular weight, and synthetic method. *J. Polym. Sci. B* **50,** 442–453 (2012).
21. Zen, A. *et al.* Effect of molecular weight on the structure and crystallinity of poly(3-hexylthiophene). *Macromolecules* **39,** 2162–2171 (2006).
22. Clark, J., Chang, J-F., Spano, F. C., Friend, R. H. & Silva, C. Determining exciton bandwidth and film microstructure in polythiophene films using linear absorption spectroscopy. *Appl. Phys. Lett.* **94,** 163306 (2009).
23. Takacs, C. J. *et al.* Remarkable order of a high-performance polymer. *Nano Lett.* **13,** 2522–2527 (2013).
24. McCulloch, B. *et al.* Polymer chain shape of poly(3-alkylthiophenes) in solution using small-angle neutron scattering. *Macromolecules* **46,** 1899–1907 (2013).
25. Spakowitz, A. J. & Wang, Z-G. Exact results for a semifexible polymer chain in an aligning field. *Macromolecules* **37,** 5814–5823 (2004).
26. Pingel, P. *et al.* Temperature-resolved local and macroscopic charge carrier transport in thin P3HT layers. *Adv. Funct. Mater.* **20,** 2286–2295 (2010).
27. Bolsée, J-C., Oosterbaan, W. D., Lutsen, L., Vanderzande, D. & Manca, J. The importance of bridging points for charge transport in webs of conjugated polymer nanofibers. *Adv. Funct. Mater.* **23,** 862–869 (2013).
28. Kondov, S. S., McGehee, W. R., Zirbel, J. J. & DeMarco, B. Three-dimensional Anderson localization of ultracold matter. *Science* **334,** 66–68 (2011).
29. Gomez-Navarro, C. *et al.* Tuning the conductance of single-walled carbon nanotubes by ion irradiation in the Anderson localization regime. *Nature Mater.* **4,** 534–539 (2005).
30. Hindeleh, A. M. & Hosemann, R. Paracrystals representing the physical state of matter. *J. Phys. C* **21,** 4155–4170 (1988).
31. Treacy, M. M. J. & Borisenko, K. B. The local structure of amorphous silicon. *Science* **335,** 950–953 (2012).
32. Rivnay, J. *et al.* Structural origin of gap states in semicrystalline polymers and the implications for charge transport. *Phys. Rev. B* **83,** 121306 (2011).
33. Poelking, C. *et al.* Characterization of charge-carrier transport in semicrystalline polymers: Electronic couplings, site energies, and charge-carrier dynamics in poly(bithiophene-alt-thienothiophene) [PBTTT]. *J. Phys. Chem. C* **117,** 1633–1640 (2013).
34. Baldo, M. A., Soos, Z. G. & Forrest, S. R. Local order in amorphous organic molecular films. *Chem. Phys. Lett.* **347,** 297–303 (2001).
35. Pasveer, W. F. *et al.* Unified description of charge-carrier mobilities in disordered semiconducting polymers. *Phys. Rev. Lett.* **94,** 206601 (2005).
36. Street, R. A., Northrup, J. E. & Salleo, A. Transport in polycrystalline polymer thin-film transistors. *Phys. Rev. B* **71,** 165202 (2005).
37. Zhang, X. *et al.* In-plane liquid crystalline texture of high-performance thienothiophene copolymer thin films. *Adv. Funct. Mater.* **20,** 4098–4106 (2010).
38. Kline, R. J. *et al.* Critical role of side-chain attachment density on the order and device performance of polythiophenes. *Macromolecules* **40,** 7960–7965 (2007).
39. Cho, E. *et al.* Three-dimensional packing structure and electronic properties of biaxially oriented poly(2,5-bis(3-alkylthiophene-2-yl)thieno-[3,2-b]thiophene) films. *J. Am. Chem. Soc.* **134,** 6177–6190 (2012).
40. Brinkmann, M. & Rannou, P. Molecular weight dependence of chain packing and semicrystalline structure in oriented films of regioregular poly(3-hexylthiophene) revealed by high-resolution transmission electron microscopy. *Macromolecules* **42,** 1125–1130 (2009).
41. Reid, O. G. *et al.* The influence of solid-state microstructure on the origin and yield of long-lived photogenerated charge in neat semiconducting polymers. *J. Polym. Sci. B* **50,** 27–37 (2012).
42. Tong, M. *et al.* Higher molecular weight leads to improved photoresponsivity, charge transport and interfacial ordering in a narrow bandgap semiconducting polymer. *Adv. Funct. Mater.* **20,** 3959–3965 (2010).
43. Kline, R. J. *et al.* Dependence of regioregular poly(3-hexylthiophene) film morphology and field-effect mobility on molecular weight. *Macromolecules* **38,** 3312–3319 (2005).
44. Troisi, A. The speed limit for sequential charge hopping in molecular materials. *Org. Electron.* **12,** 1988–1991 (2011).
45. DeLongchamp, D. M. *et al.* Controlling the orientation of terraced nanoscale ribbons of a poly(thiophene) semiconductor. *ACS Nano* **3,** 780–787 (2009).
46. Rivnay, J., Noriega, R., Kline, R. J., Salleo, A. & Toney, M. F. Quantitative analysis of lattice disorder and crystallite size in organic semiconductor thin films. *Phys. Rev. B* **84,** 045203 (2011).


## Acknowledgements

We thank G. Rumbles for his comments in the preparation of this manuscript. We gratefully thank A. Facchetti and Z. Chen (Polyera, Skokie, IL), and I. McCulloch and M. Heeney (Imperial College, London) for supplying materials (P[NDI2OD-T2], P3HT, and PBTTT). This work is supported by the Center for Advanced Molecular Photovoltaics Award No. KUS-C1-015-21 made by King Abdullah University of Science and Technology (KAUST) (R.N., J.R., K.V., A.S.), and NSF (J.R., A.S.). N.S. acknowledges support by a European Research Council (ERC) Starting Independent Researcher Fellowship under the grant agreement No. 279587. Portions of this research were carried out at the Stanford Synchrotron Radiation Lightsource, a national user facility operated by Stanford University on behalf of the US Department of Energy, Office of Basic Energy Sciences.

## Author contributions

A.S., J.R. and R.N. conceived the research. J.R., R.N., K.V. and F.P.V.K. prepared samples for optoelectronic and structural measurements. J.R. and R.N. carried out the XRD experiments and analysed the data. R.N. and K.V. performed the electrical and optical measurements. R.N. performed the simulations. M.F.T., P.S. and N.S. assisted with data interpretation. R.N., J.R. and A.S. wrote the manuscript and all authors participated in manuscript preparation and editing.

## Additional information

Supplementary information is available in the online version of the paper. Reprints and permissions information is available online at www.nature.com/reprints. Correspondence and requests for materials should be addressed to A.S.

## Competing financial interests

The authors declare no competing financial interests.

nature materials

SUPPLEMENTARY INFORMATION

DOI: 10.1038/NMAT3722

# A general relationship between disorder, aggregation and charge transport in conjugated polymers

*Rodrigo Noriega*[+,1,†], *Jonathan Rivnay*[+,2,§], *Koen Vandewal*[2], *Felix P.V. Koch*[3], *Natalie Stingelin*[3,4], *Paul Smith*[3], *Michael F. Toney*[5], and *Alberto Salleo*[2*]

[1] Dept. of Applied Physics, Stanford University, Stanford CA

[2] Dept. of Materials Science and Engineering, Stanford CA

[3] Dept. of Materials, ETH Zurich, Zurich (Switzerland)

[4] Dept. of Materials and Centre of Plastic Electronics, Imperial College London (UK)

[5] Stanford Synchrotron Radiation Lightsource (SSRL), SLAC National Accelerator Laboratory, Menlo Park, CA

[+] Contributed equally to this work.

[*] To whom correspondence should be addressed. Email: asalleo@stanford.edu.

[†] Current address: Department of Chemistry, University of California Berkeley.

[§] Current address: Department of Bioelectronics, Ecole Nationale Supérieure des Mines de Saint-Étienne.

DOI: 10.1038/NMAT3722

## Supplementary Methods and Discussion

## I. Typical packing structure of semicrystalline polymers

Semicrystalline polymers interact to form π-stacks and side chain lamellar stacks, which result in short-range aggregates or long-range crystallites depending on the molecular structure of the polymer, processing conditions and the strength of such interactions. A typical material described in the main text, PBTTT, forms remarkably well ordered lamellar stacks in the direction normal to the substrate when cast onto thin films, in a classic example of what is called "edge-on" texture (Fig. S1). The stacking along the π-π direction is much more disordered and lies preferentially along the plane of the substrate, as does the backbone repeat. These two directions (π-π and backbone) are the most relevant for charge transport, with the π-stacks being the most important for intermolecular charge transfer.

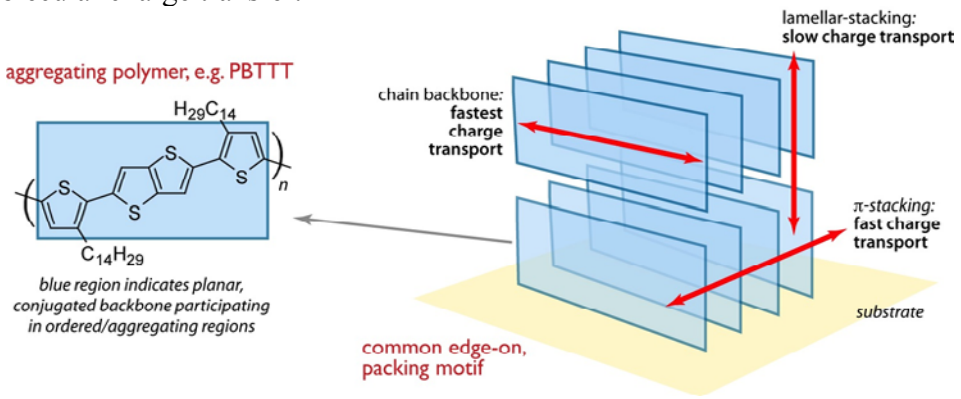


**Fig. S1.** Typical π-π edge-on packing observed for classic semicrystalline polymers. The three main charge transport directions are shown.

## II. Comparing the optoelectronic properties of regio-random P3HT and the amorphous fraction of regio-regular P3HT

The absorption spectrum of a semicrystalline polymer is composed of two overlapping components: the contributions from the aggregate fraction and that from the amorphous fraction. It has been shown previously that the optical absorption/emission of the aggregate fraction is described with a Franck-Condon model coupling electronic transitions and nuclear vibrations. Such vibronic progression is the product of a collection of co-facial aggregates.[1-4] Interestingly, if one subtracts the Franck-Condon vibronic progression due to the aggregates, the residual absorption matches that of the polymer in solution and is therefore assigned to the amorphous polymer phase in the film.

We compare the optical absorption spectrum from such amorphous phase in a regio-regular (RR), semicrystalline, P3HT film to that of a regio-random (RRa) P3HT sample (Fig. S2). Here, the optical absorption spectra were obtained with a combination of conventional UV-vis spectroscopy for the strong absorption regions and photothermal deflection spectroscopy (which has a higher sensitivity) for the low absorption regions.[5] The similarity between the two absorption spectra is clear in the part assigned to HOMO-LUMO transitions (E> 2.2 eV). Hence we conclude that RRa-P3HT constitutes a good model of the amorphous phase present in RR-P3HT films. Also, the regio-random film has very few other deep states in the bandgap. We conclude that the electronic structure of the amorphous phase present in the RR-P3HT film does not have states extending in

DOI: 10.1038/NMAT3722

the bandgap of the aggregate phase in RR-P3HT. Therefore, we can approximate the energy levels of the amorphous fraction of the regio-regular film as that of a regio-random sample, and thus elucidate the charge transport at the interface between the amorphous and aggregated fractions of a RR-P3HT film.[6]

The energy levels obtained for films of regio-regular and regio-random films with cyclic voltammetry are $E^{RR}$=4.99 eV and $E^{RRa}$=5.25 eV, respectively.[7] Thus, a hole would need to overcome a barrier of 260 meV (~10 kT at room temperature) to hop from an aggregate to an amorphous region in semicrystalline P3HT. If the hole were to transfer to a state with a similar energy position to $E^{RR}$, it would need to find a state deep in the tail of the DOS of the amorphous region (about twice the tail energetic breadth) and be located close to an interface between crystalline and amorphous regions. Due to the low population of states in the amorphous phase at such energy (Fig. S2) and the strongly localized nature of deep tail states (Fig. 3), the hole would not be able to escape the interface, and would likely hop back to the aggregate region, where there are significantly more accessible states.

The presence of polaronic effects could weaken the assertion that holes remain in the P3HT aggregates. Indeed, Street et al.[6] estimated that the band offset between amorphous and crystalline regions in P3HT (~0.3 eV) is approximately equal to the polaron binding energy difference in the two regions. Quantifying experimentally polaronic effects is extremely challenging. Nevertheless, in the next Section we show experimental proof that charges do remain confined in the aggregates in P3HT films. Hence, we can confidently state that polaronic effects do not induce charge leakage from the aggregates into the amorphous regions of P3HT.

Optical measurements probe the energy required to create neutral excitations, and are determined by the details of the electronic states in the system, as well as by the nature of such excitations (localized vs. delocalized) and its interactions with the lattice (reorganization energy). It should be noted that the optical measurements presented here (Fig. S2) are intended to be an indication of the existence of a large energetic offset between the crystalline and amorphous regions of the film. The effect of energetic offset on transport is addressed by our electroluminescence experiments, described in the following section.

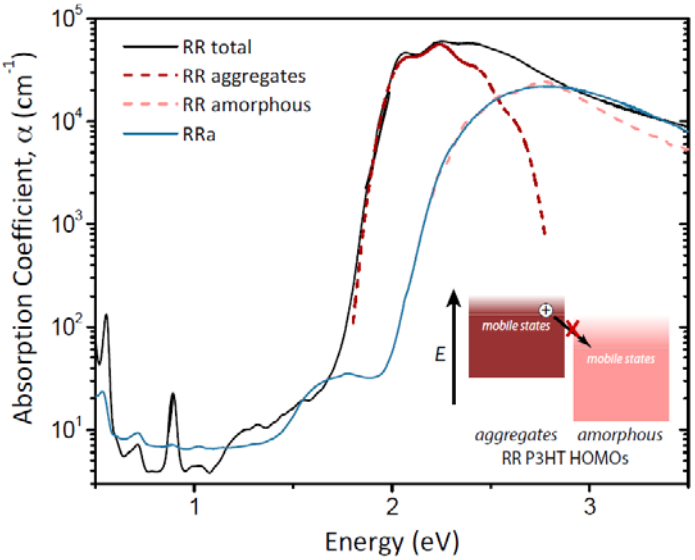


**Fig. S2.** Absorption spectra of RR- and RRa-P3HT films. The semicrystalline (RR) P3HT presents two components: a vibronic progression from co-facial aggregates and a larger bandgap, featureless absorption from the amorphous fraction of the film. Amorphous (RRa) P3HT shows a single component in its spectrum, matching that of the amorphous fraction of RR-P3HT.

**III. Motion of charges in films with varying amounts of aggregated material**

Films made of blends of RRa-P3HT and RR-P3HT pre-aggregated in a solution mixture represent a model system to study the motion of charges in films of semicrystalline polymers. Device fabrication and electro-optical characterization details are presented in the Methods section. The electroluminescence (EL) and photoluminescence (PL) spectra for these devices were collected using a cooled CCD camera and corrected for the spectrometer response. Photoluminescence experiments used a pump beam from a 535 nm diode laser. RR-P3HT and RRa-P3HT devices required a different amount of current to exhibit a measurable signal due to varying luminescence yields. As expected, the EL and PL signals for each of these films made from pure materials agree well with each other (Fig. S3).

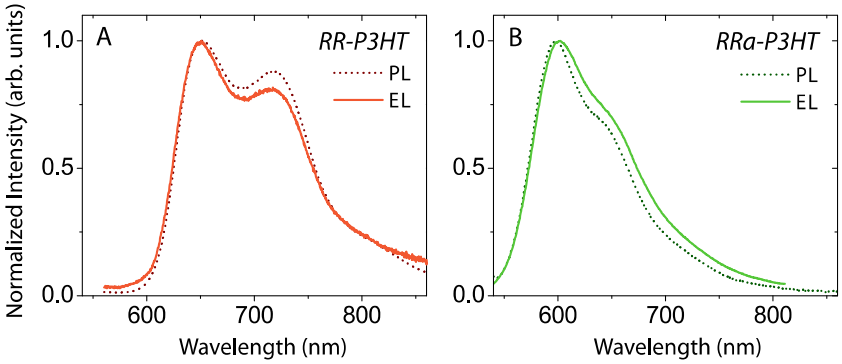


**Fig. S3.** Photoluminescence and electroluminescence spectra for films of pure RR- and RRa-P3HT spun cast from dichlorobenzene.

DOI: 10.1038/NMAT3722

To vary the amount of aggregated material in the films, the starting solutions of RR- and RRa-P3HT in DCB were diluted with ethylacetate (2:1 DCB:EtOAc solvent ratio) to form the stock solutions for pre-aggregated and amorphous materials, which were then mixed in 1:1 and 1:9 ratios. Hence, the solvent mixture and material concentration remained constant for all samples. Films from solutions containing 100%, 50%, and 10% pre-aggregated material were spun cast onto ITO/PEDOT films and the diode structures were completed with evaporated Ca/Al electrodes to form devices with an area of 0.1 $cm^2$. Photoluminescence and electroluminescence experiments were performed as described above. EL spectra were collected for different values of current for each device (Fig. S4.).

For the film with the maximum amount of aggregated material - made from the solution containing only RR-P3HT in DCB/EtOAc – the PL and EL spectra (Fig. S4B) are almost identical to the results obtained with the sample cast from RR-P3HT in DCB. The film with 50% pre-aggregated material shows practically the same results, with a slight change in the relative intensities of the 0-0 and 0-1 peaks. Most importantly, there is no signal from the amorphous regions in either the PL or EL – even at high currents – for either of these samples. These observations can be explained by the large amount of aggregates in both films, allowing charges to be injected in and transported through an interconnected network of aggregates, and at the same time allowing any excitons formed in the amorphous regions to migrate to the lower-bandgap aggregates efficiently via energy transfer.

Interestingly, the sample with 10% pre-aggregated material in 90% RRa-P3HT (Fig. S4D) shows a different behavior. Its PL signal contains the signature of aggregated and amorphous material, but the EL spectra at low currents show only the emission from aggregates. Increasing the current in the device causes the appearance of an additional weak feature in the EL signal, in a position matching the emission from amorphous P3HT as observed in the RRa-P3HT sample. After the appearance of the new feature due to charge recombination in the amorphous regions, further increase of the current causes this component of the EL spectrum to be more pronounced. Since the electroluminescence shows only the signature of aggregate emission, but the photoluminescence displays a combination of emission from amorphous and aggregated material, we conclude that the electroluminescence spectra are due exclusively to recombination within the aggregates and not to exciton energy transfer to the aggregates prior to recombination. We interpret these results as evidence that charge transport is most favorable in the ordered regions of semicrystalline films, and if an interconnected network of aggregates is present then charges will move almost exclusively through such a network without significant excursions into the surrounding amorphous material. If the amount of charge in the sample is large enough to saturate the ordered regions—or to cause Coulombic repulsion to raise the energy levels of the aggregates to match those of the amorphous regions—then charges move through the amorphous and ordered regions of the film. It should be noted that the current density where emission from the amorphous regions starts becoming relevant (~100 $mA/cm^2$) is much higher than that usually encountered in organic electronic devices.

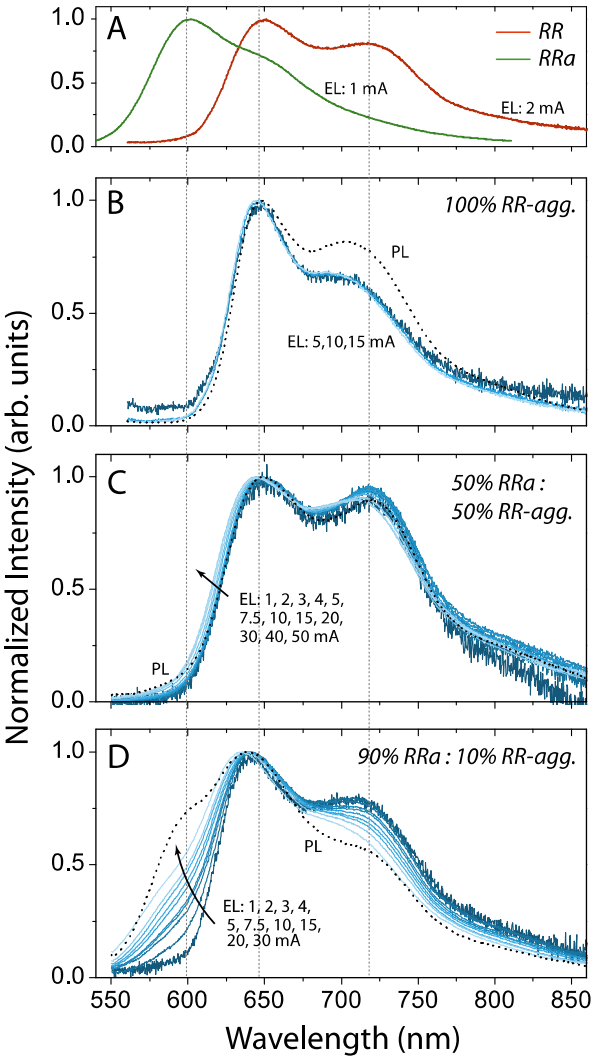


**Fig. S4.** Photoluminescence and electroluminescence of films made from blends (in solution) of RRa-P3HT and pre-aggregated RR-P3HT. (A) Reference electroluminescence spectra from pure RR and RRa P3HT. (B-D) Photoluminescence spectra for each film is shown in black (dotted), along with electroluminescence spectra for increasing values of current in the devices. The film composition (aggregates vs. RRa matrix) is indicated in each panel. Vertical dashed lines are the EL peak positions for the amorphous, and 0-0, 0-1 aggregate transitions of the pristine films. Panels A and D of this figure are also in Fig. 2 in the main text.

These results point to the fact that an interconnected network of aggregates supports charge transport in high molecular weight semicrystalline polymers. Since aggregates must be connected by polymer chains, it is useful to expand on such bridging mechanism.

The simplest way to estimate the separation between aggregates is assuming a 2D model with infinitely-long aggregates along the π-stacking direction, so the aggregate fraction corresponds to the ratio of the aggregate length along the backbone and the space filled

DOI: 10.1038/NMAT3722

with amorphous material. The length of aggregates along the backbone direction can be estimated by using the exciton bandwidth calculated from the absorption spectrum and matching it to simulations. Increasing the aggregate length delocalizes the exciton along each chain, decreasing its interchain character and lowering the exciton bandwidth. Turner et al.[8] used this model to calculate the spacing between aggregates in P3HT. Infinite and perfectly oriented π-stacks are not an accurate representation of the polymer microstructure as discussed in the rest of this work, but provide an initial approximation for the polymer length that could bridge aggregates.

Using reasonable values from the literature,[8] we can estimate the distance between P3HT aggregate domains. In a film made of ~40% aggregates with a size of 10-20 nm along the polymer backbone, the distance between edges of adjacent aggregates will be ~15 nm. The persistence length of P3HT is ~2.4-3.3 nm[9-11] which means that a bridging chain only needs to traverse a few persistence lengths between the edges of two aggregates (where its orientation is fixed) without incurring a drastic orientation change. More importantly, a P3HT chain of MW~17-24 kg/mol would be sufficient to bridge two nearest-neighbor aggregates, a value consistent with the transition region observed in Fig. 4 of the main text.

## IV. Estimate of the melting enthalpy of a P3HT paracrystal

A perfectly-ordered crystal corresponds to the molecular arrangement that minimizes—either globally, or locally in the case of metastable polymorphs—the system's energy. Introducing distortions will prevent the system from reaching that energetically-favorable configuration and thus increase the disordered crystal's energy relative to the perfect crystal. This energetic difference must be taken into account when analyzing the properties of such systems (e.g. melting enthalpy) since phase transformations do not start from the perfect crystal state.

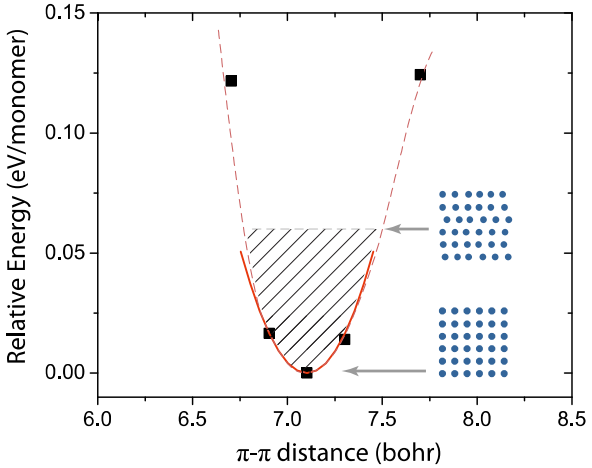


**Fig. S5.** The change in energy of a system with disorder will affect its thermal properties. Distortions in the lattice positions raise the relative energy of the system and will reduce its melting enthalpy. Here, the effect of disorder in the π-π stacking of P3HT on the crystal energy—normalized per monomer—are shown, along with a quadratic fit (solid

red line), and two schematic representations of low and high amounts of disorder. Data points (black squares) were obtained with density functional theory simulations[12].

Shown in Fig. S5 is the relative change in energy of a P3HT crystal upon distortions of the π-π stacking distance around the equilibrium value of $d_o$=7.1 bohr (~3.76 Å). We can use this information to estimate the change in the melting enthalpy for a P3HT crystal disordered in the π-π stacking direction, with lattice spacings following a normal distribution about the equilibrium value with a variance $s^2 = d^2 g^2$. To calculate the relative energy of the crystal $dE$, we can approximate its dependence as a parabola with a minimum at $d=d_0$. Normalizing the distortions by $d_0$, $x=(d-d_0)/d_0$, we can write $dE=Ax^2$. The average value will depend on the probability distribution of $x$, so for a Gaussian distribution (as in the paracrystalline model) we get

$$\langle dE \rangle = A\langle x^2 \rangle = As_x^2 = Ag^2 \qquad \text{Eq. S1.}$$

A quadratic fit to the data of Fig. S5 yields $A$~21 eV/monomer. For a P3HT monomer with mass $M_m$~3x10$^{-22}$ grams, the melting enthalpy is

$$H_m = H_o - dH = H_o - \frac{A \cdot g^2}{M_m} \approx 99\,{}^{J}\!/_{g} - \frac{21\,{}^{eV}\!/_{monomer} \cdot g^2}{3 \cdot 10^{-22}\,{}^{g}\!/_{monomer}} 1.6 \cdot 10^{-19}\,{}^{J}\!/_{eV} \qquad \text{Eq. S2.}$$

Where $H_0$ is the melting enthalpy of a perfect crystal. A commonly-accepted value for $H_0$ is 99 J/g.[13] With this simple estimate, a paracrystal with $g$=7% will have a melting enthalpy of $H_m$~45 J/g. While this is a semi-quantitative model of the experimentally-accessible melting enthalpy, it shows that in real thin films, the melting enthalpy can be much less than in perfect crystals. Calorimetry data can thus be interpreted as describing a film having a high density of disordered crystallites rather than a low-density of perfect crystallites. This is relevant since overlapping elliptical aggregates with an aspect ratio of 10 can form a 2D (3D) percolating network when their volume fraction is only 30% (8.7%).[14]

## V. Measurement of lattice disorder

To decouple size and disorder effects from the diffraction profile of organic semiconductors, we utilize a technique first developed by Warren and Averbach,[15-17] but perform a full fit to the data and include error propagation to provide confidence in the analysis results.[18] Importantly, especially for polymers, it is prudent to crystallographically align the thin film, so as to separate diffracted intensity from different crystallographic directions, and to increase the collection of diffracted intensity from weakly scattering systems.

Broadening of XRD peaks arises from a diffraction-order-independent component related to crystallite size, and a diffraction-order-dependent portion due to cumulative disorder that includes paracrystallinity and variations in the average lattice spacing.[15] Paracrystalline disorder is a cumulative, static statistical fluctuation of local lattice spacings. It is described by a parameter $g$, the reduced variance in the separation between planes along a given crystallographic direction.[19,20] The anisotropic nature of disorder in semicrystalline polymers, as well as the reduced disorder in small molecule crystals can

DOI: 10.1038/NMAT3722

be observed in the parameters obtained for PBTTT and TIPS-Pn, shown in Table S1. Importantly, one notes the predominant role of paracrystallinity in semicrystalline polymers.

**Table S1.** Warren Averbach full fit results for PBTTT and TIPS pentacene along directions perpendicular to the substrate plane, and in one direction parallel to the substrate (relevant for charge transport).

| ***Material*** | ***Diffraction geometry, crystallographic direction*** | ***M (nm)*** | ***g (%)*** | $e_{RMS}$ ***(%)*** |
|---|---|---|---|---|
| PBTTT | *Specular*, Lamellar stacking [100] | 34 ± 7 | 2.6 ± 1.4 | 1.3 ± 0.6 |
| | *Grazing*, π-stacking [010] | n/a | 7.3 ± 0.7 | 0.9 ± 0.6 |
| TIPS-Pentacene | *Specular*, ***c*** [001] | 55 ± 8 | ~0 | ~0 |
| | *Grazing*, ***a*** [100] | 47 ± 7 | 0.9 ± 0.6 | ~0 |

**VI. Validation of the single-peak estimate for paracrystalline disorder**

In order to perform the full analysis as in the previous section (described in Ref.[18]), multiple diffraction orders are necessary. However, this type of data is difficult to obtain in materials that are strongly disordered in the crystallographic direction of interest (such as the π-π stacking direction), if it is found in the substrate plane. In this section we describe an estimation of disorder using a single peak-width, and validate it as a largely accurate -and if inaccurate slightly conservative- estimate of disorder.

It is possible to obtain a single peak-width estimation of disorder using only the center position ($q_o$) and breadth ($\Delta_q$) of a diffraction peak:[18]

$$g = \sqrt{\frac{\Delta_q}{2\pi q_0}}. \qquad \text{Eq. S3.}$$

This estimate is accurate if two assumptions are valid. First, the XRD peak width and shape are entirely described by cumulative disorder. Under this assumption the role of the column length (generally considered a metric of grain size) is negligible—a reasonable assumption given the results for PBTTT in Table S1 and Ref.[18]. Second, paracrystallinity is more significant than lattice parameter fluctuation. In this section we provide arguments to sustain that both assumptions are valid. We focus on polymers with thiophene-based moieties, especially those used to obtain high performance. In higher MW polymers, a second order π-stacking peak is rarely observed; in PBTTT alignment techniques were required to properly resolve the (020) peak. In fact, many structural investigations of PBTTT have suggested that this polymer displays an unprecedented amount of qualitative 'order.'[21-23] In comparison, other polymers in the literature show no

such qualitative order, and must therefore be *no more ordered than PBTTT*, and at best, as ordered as PBTTT. Furthermore, in polymer π-stacking the contribution of paracrystalline disorder is found to consistently dominate over lattice parameter fluctuation (see, for example, Table S1). Thus, Eq. S3 provides an appropriate estimate of the paracrystallinity of other high molecular weight polymer systems.

To test whether the single-peak estimate is a valid approximation in the low MW regime, a 13-monomer chain of 3-hexylthiophene was used to measure the diffraction peaks associated with the commonly observed polymer phase, or Form I of P3HT. Given the increasing trend of $g$ with MW, if we find that the single-peak estimate is valid at low MW, its validity is even stronger at high MW. Grazing incidence X-ray scattering data was collected at beamline 7-2 of the Stanford Synchrotron Radiation Lightsource. A Lorentz correction to the detected intensity was necessary due to the experimental geometry, and the corrected data for each peak was described with a pseudo-Voigt lineshape and a flat background (Fig. S6A). Since second-order peaks are more sensitive to intensity and shape changes due to damage by the X-ray beam during measurement, initial scans to select the regions of reciprocal space that would later be studied in detail were performed, then the sample was moved so that a fresh spot was under illumination for each following scan. To verify the absence of beam damage, data from two fresh spots in the sample was compared to data taken after significant beam exposure (Fig. S6B)

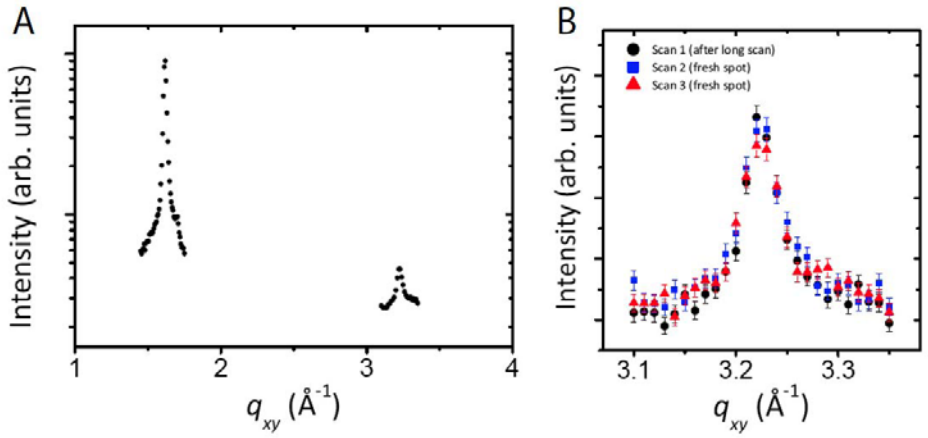


**Fig. S6**. (A) Lorentz-corrected diffraction pattern for the first and second order diffraction peaks of the π-π stacking direction of Form I P3HT in a 13-monomer long chain of 3-hexylthiophene. (B) Multiple scans on the second order π-stacking peak to verify minimal damage due to X-rays.

A complete peak shape analysis (Fig. S7) on the two detected diffraction peaks for the P3HT (13 monomer) oligomer was performed and compared to the single peak estimation for the same data set. Due to weak scattering from these films and a propensity for beam damage, a low measurement point density was used and only a narrow range of reciprocal space was explored around each peak, at the expense of a broader range with higher point density needed to increase the confidence in the fitting analysis. We observe that the single-peak estimate for the paracrystalline disorder is an overestimation not surprising for a semi-ordered material as the P3HT oligomer ($g_{single}$=4.7%,

DOI: 10.1038/NMAT3722

$g_{full}$=2.7±0.6%). This overestimation is caused by neglecting the effects of a finite grain size ($M_{full}$~18 nm), which necessarily occurs in the single-peak estimate of $g$. Thus for Figure 4 in the main text, the estimates of $g$ we give for the oligomers are high: P3HT oligomers are likely more ordered than we show, making the transition between high and low MW even more pronounced. For higher MW samples with increasing amounts of disorder, the effects of a finite grain size disappears and the single-peak estimate will be closer to the actual value for $g$. To prove this point, the agreement of the $g$ estimated in PBTTT using single-peak data from Chabinyc and co workers,[21] with that calculated from a full WA analysis of PBTTT (Fig. 4, main text) is excellent.

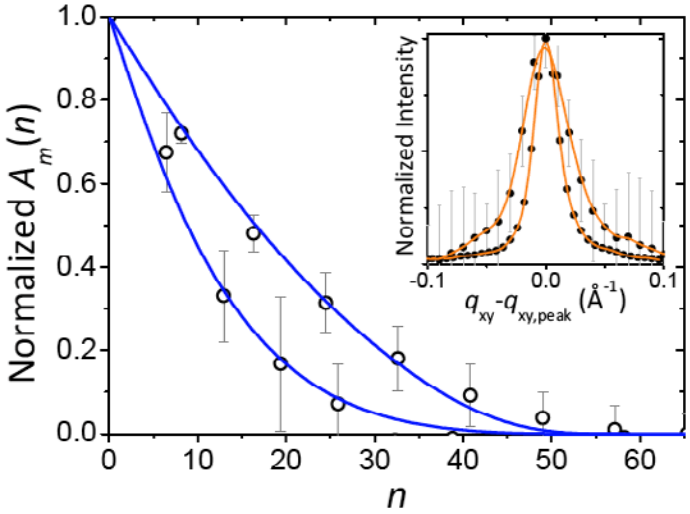


**Fig. S7.** Fourier transform of the diffraction peaks and the corresponding fits to a Warren-Averbach model. Inset: Peak shapes for the first and second order diffraction peaks of a P3HT oligomer, normalized and centered at the maximum of each peak to observe order-dependent broadening.

## VII. Differences in diffraction patterns as a result of disorder in a polymer film

2D grazing incidence X-ray diffraction (2D-GIXD) experiments on thin films (Fig. S8) are useful to observe how disorder affects the diffraction pattern of polymer samples, as measured in several of the materials discussed in this work. This comparison will be helpful in understanding the differences between a fully amorphous microstructure and a semicrystalline one, as well as to illuminate the nature of polymers that are disordered but still retain local order.

The evolution of the diffraction patterns with increasing amounts of disorder is evident, from well defined spots and streaks corresponding to a 3D ordering characteristic of classic semicrystalline samples (top Fig. S8, see also Fig. S1) to the broad, featureless scattering of completely amorphous materials (bottom Fig. S8). Semicrystalline samples are not only the most ordered, but also commonly the most textured. The often cited "amorphous hump" assigned to flexible alkyl chains (q~1.4Å$^{-1}$) is dominant in disordered materials, but also present in the background for semicrystalline polymers with disordered side chains (as opposed to the well-ordered interdigitating side chains of PBTTT, for example).

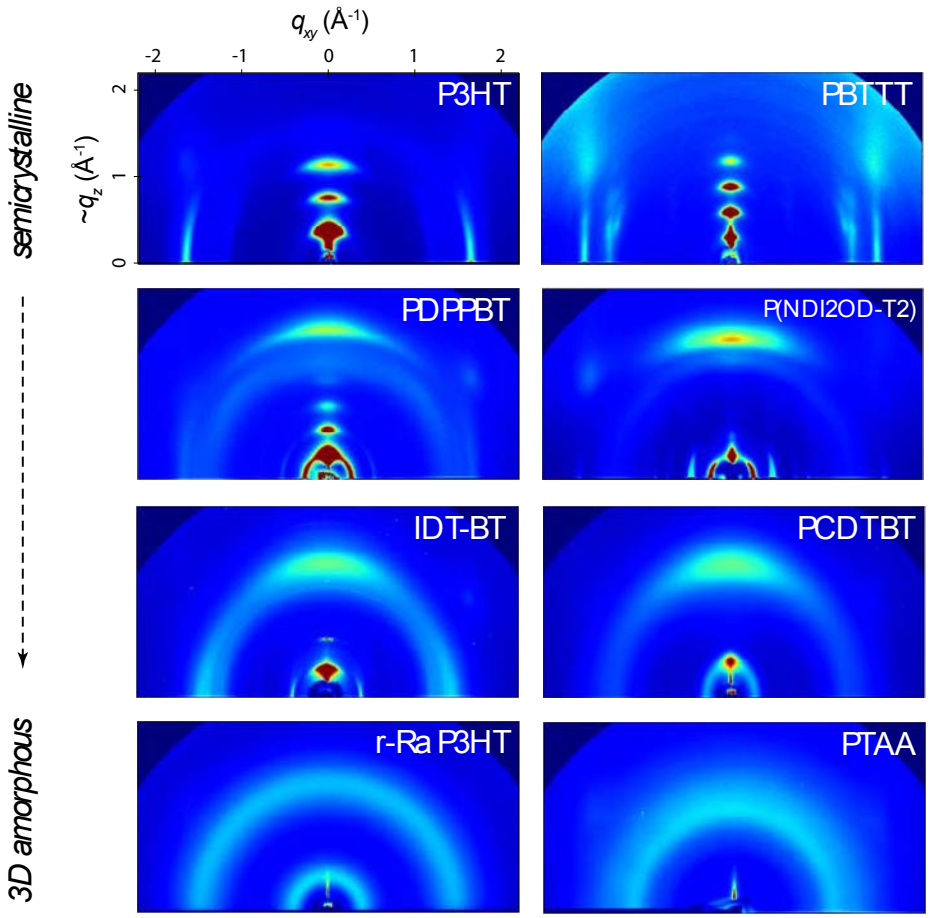


**Fig. S8.** 2D-GIXD for a collection of polymers with various amounts of disorder. From top left to bottom right: High MW bar-coated P3HT, spun cast PBTTT-C14 annealed at 180°C, spun cast PDPPBT annealed at 200°C, spun cast P(NDI2OD-T2) annealed at 150°C, IDT-BT from Ref.[24], spun cast PCDTBT, spun cast regio-random P3HT, and spun cast PTAA. These measurements were performed at the Stanford Synchrotron Radiation Lightsource beamline 11-3, with an X-ray energy of 8 keV and an incidence angle of 0.1º.

Between these two extremes we find a transition, where some of the recent top performing materials lie. In this gray area between semicrystalline and fully 3D amorphous microstructures, disorder progressively destroys long range correlations. However, this transition from long range to short range order happens anisotropically, since the bulky macromolecular units that make up the paracrystals interact differently in each stacking direction (for example, π-π interactions are weaker than alkyl stacking in polymers with interdigitating side chains like PBTTT). For example, PDPPBT and P(NDI2OD-T2) exhibit a broad and semi-textured π-stacking peak out of plane (Fig. S8) and noticeable scattering from both alkyl and backbone repeat planes, while more disordered polymers like PCDTBT and IDT-BT display an even broader and less textured π-stacking peak but little, if any, diffracted intensity from other stacking directions.

DOI: 10.1038/NMAT3722

## VIII. Sources used for *g* estimates, mobility and activation energy (Figs. 4, 5)

***Figure 4.***


a. R. J. Kline *et al.*, *Macromolecules* **38**, 3312 (2005).
b. M. L. Chabinyc, M. F. Toney, R. J. Kline, I. McCulloch, M. Heeney, *Journal of the American Chemical Society* **129**, 3226 (2007).
c. L. H. Jimison, A. Salleo, M. L. Chabinyc, D. P. Bernstein, M. F. Toney, *Physical Review B* **78**, (2008).
d. J. T. Rogers, K. Schmidt, M. F. Toney, E. J. Kramer, G. C. Bazan, *Advanced Materials* **23**, 2284 (2011).
e. This work, and J. Rivnay *et al.*, *Macromolecules* **44**, 5246 (2011).
f. J. Guo *et al.*, *The Journal of Physical Chemistry B* **114**, 742 (2009).
g. H. Chen et al., Advanced Materials 24, 4618 (2012).
h. J. Mei, D. H. Kim, A. L. Ayzner, M. F. Toney, Z. Bao, *Jornal of the American Chemical Society* **133**, 20130 (2011).
i. A. J. Kronemeijer *et al.*, *Advanced Materials* **24**, 1558 (2012).
j. N. Reitzel *et al.*, *Journal of the American Chemical Society* **122**, 5788 (2000).
k. C. M. Zimmerman, W. J. Koros, *Polymer* **40**, 5655 (1999). (*molecular weight estimate from viscosity)
l. R. J. Kline, M. D. McGehee, E. N. Kadnikova, J. Liu, J. M. J. Fréchet, *Advanced Materials* **15**, 1519 (2003).
m. A. Zen *et al.*, *Advanced Functional Materials* **14**, 757 (2004).
n. A. Zen *et al.*, *Macromolecules* **39**, 2162 (2006).
o. J.-F. Chang *et al.*, *Physical Review B* **74**, 115318 (2006).
p. R. Zhang *et al.*, *Journal of the American Chemical Society* **128**, 3480 (2006).
q. J.-M. Verilhac *et al.*, *J. Phys. Chem. B* **110**, 13305 (2006).
r. J.-H. Huang *et al.*, *Organic Electronics* **12**, 1755 (2011).
s. H. Yan *et al.*, *Nature* **457**, 679 (2009)
t. H. N. Tsao *et al.*, *Journal of the American Chemical Society* **133**, 2605 (2012).


***Figure 5, by material.***

Poly(2,5-bis(3-tetradecylthiophen-2-yl)thieno[3,2,-b]thiophene), PBTTT:


C. C. Wang *et al.*, *Advanced Materials* **22**, 697 (Feb, 2010).
M. J. Lee *et al.*, *Advanced Functional Materials* **21**, 932 (2011).
X. Zhang *et al.*, *Advanced Functional Materials* **20**, 4098 (2010).
S. Wang *et al.*, *Applied Physics Letters* **93**, 162103 (2008).
N. Zhao *et al.*, *Advanced Materials* **21**, 3759 (2009).


Poly[5,5′-bis(3-alkyl-2-thienyl)-2, 2′-bithiophene], PQT:


R. A. Street, J. E. Northrup, A. Salleo, *Physical Review B* **71**, 165202 (2005).
A. Salleo *et al.*, *Physical Review B* **70**, (2004).


Regio-regular poly(3hexylthiophene), P3HT:


R. J. Kline *et al.*, *Macromolecules* **38**, 3312 (2005).
L. H. Jimison, M. F. Toney, I. McCulloch, M. Heeney, A. Salleo, *Advanced Materials* **21**, 1568 (2009).
H. Sirringhaus *et al.*, *Nature* **401**, 685 (1999).

J. A. Merlo, C. D. Frisbie, *Journal of Polymer Science Part B: Polymer Physics* **41**, 2674 (2003).
J.-F. Chang, H. Sirringhaus, M. Giles, M. Heeney, I. McCulloch, *Physical Review B* **76**, 205204 (2007).
B. H. Hamadani, D. Natelson, *Applied Physics Letters* **84**, 443 (2004).
S. Ukai, H. Ito, K. Marumoto, S.-i. Kuroda, *Journal of the Physical Society of Japan* **74**, 3314 (2005).

Poly(3,3′′-di-n-decylterselenophene) , PSSS:
Z. Chen *et al.*, *Physical Review B* **84**, 115211 (2011).

Poly(5′,5′′-bithiophene-alt-2,6-[(1,5-didecyloxy)naphthalene]), PBDN:
D. S. Chung *et al.*, *Chemistry of Materials* **21**, 5499 (2009).

Diketopyrrolopyrrole-benzothiadiazole copolymer (DPP-BT), and a selenophene-based derivative (PSeDPPBT):
Y.Park, *High-k dielectric layers and their application in organic electronics*, Ph.D. dissertation, Dec. 2012.
A. J. Kronemeijer *et al.*, *Advanced Materials* **24**, 1558

Poly{[N,N-9-bis(2-octyldodecyl)naphthalene-1,4,5,8-bis(dicarboximide)-2,6-diyl]-alt-5,59-(2,29-bithiophene)}, P(NDI-T2):
This work, and J. Rivnay *et al.*, *Macromolecules* **44**, 5246 (2011).
M. Caironi *et al.*, *Advanced Functional Materials* **21**, 3371 (2011).

Poly[N-9′′-hepta-decanyl-2,7-carbazole-alt-5,5-(4′,7′-di-2-thienyl-2′,1′,3′-benzothiadiazole)], PCDTBT:
Z. M. Beiley *et al.*, *Advanced Energy Materials* **1**, 954 (2011).

Poly[(9,9-dioctylfluorenyl-2,7-diyl)-co-bithiophene], F8T2:
J. Veres, S. D. Ogier, S. W. Leeming, D. C. Cupertino, S. Mohialdin Khaffaf, *Advanced Functional Materials* **13**, 199 (2003).
M. C. Hamilton, S. Martin, J. Kanicki, *Chemistry of Materials* **16**, 4699 (2004).

Poly(triarylamine), PTAA:
J. Veres, S. D. Ogier, S. W. Leeming, D. C. Cupertino, S. Mohialdin Khaffaf, *Advanced Functional Materials* **13**, 199 (2003).

Poly(p-phenylene vinylene) derivatives, PPVs:
C. Tanase, E. J. Meijer, P. W. M. Blom, D. M. de Leeuw, *Physical Review Letters* **91**, 216601 (2003).
D. E. Markov, C. Tanase, P. W. M. Blom, J. Wildeman, *Physical Review B* **72**, 045217 (2005).
A. J. Campbell, D. D. C. Bradley, E. Werner, W. Brütting, *Synthetic Metals* **111-112**, 273 (2000).

DOI: 10.1038/NMAT3722

C. Im, H. Bassler, H. Rost, H. H. Horhold, *The Journal of Chemical Physics* **113**, 3802 (2000).
M. M. Mandoc, B. de Boer, G. Paasch, P. W. M. Blom, *Physical Review B* **75**, 193202 (2007).
H. C. F. Martens, P. W. M. Blom, H. F. M. Schoo, *Physical Review B* **61**, 7489 (2000).
W. F. Pasveer *et al.*, *Physical Review Letters* **94**, (2005).

Regio-random poly(3hexylthiophene), RRa-P3HT:
S. Ukai, H. Ito, K. Marumoto, S.-I. Kuroda, *Journal of the Physical Society of Japan* **74**, 3314 (2005).

## IX. Charge transport measurements on a representative subset of thin P3HT films of different molecular weights

Here we provide a representative subset of the electrical properties of thin film field-effect transistors made from P3HT of varying molecular weight. The drain current ($I_d$) as a function of gate voltage ($V_g$) is displayed in the transfer curves (Fig. S9.A). We also show the mobility as a function of molecular weight for these samples (Fig. S9.B).

While the use of techniques which probe bulk charge transport to directly relate X-ray scattering and electrical techniques is desirable, such measurements (e.g. time-of-flight or space charge limited current) operate in a low charge carrier density regime. Here the charge mobility depends more strongly on a larger set of microstructural factors that are less important for high charge density transistor measurements. Nevertheless, thickness dependent studies[25,26] have shown that the coherence length of π-stacking in polythiophene films is invariant as the film thickness decreases from hundreds of nanometers to highly confined films of only a few nanometers. Thus, our use of bulk scattering techniques (where we measure diffraction peak widths) to link transport in transistors to film microstructure is justified.

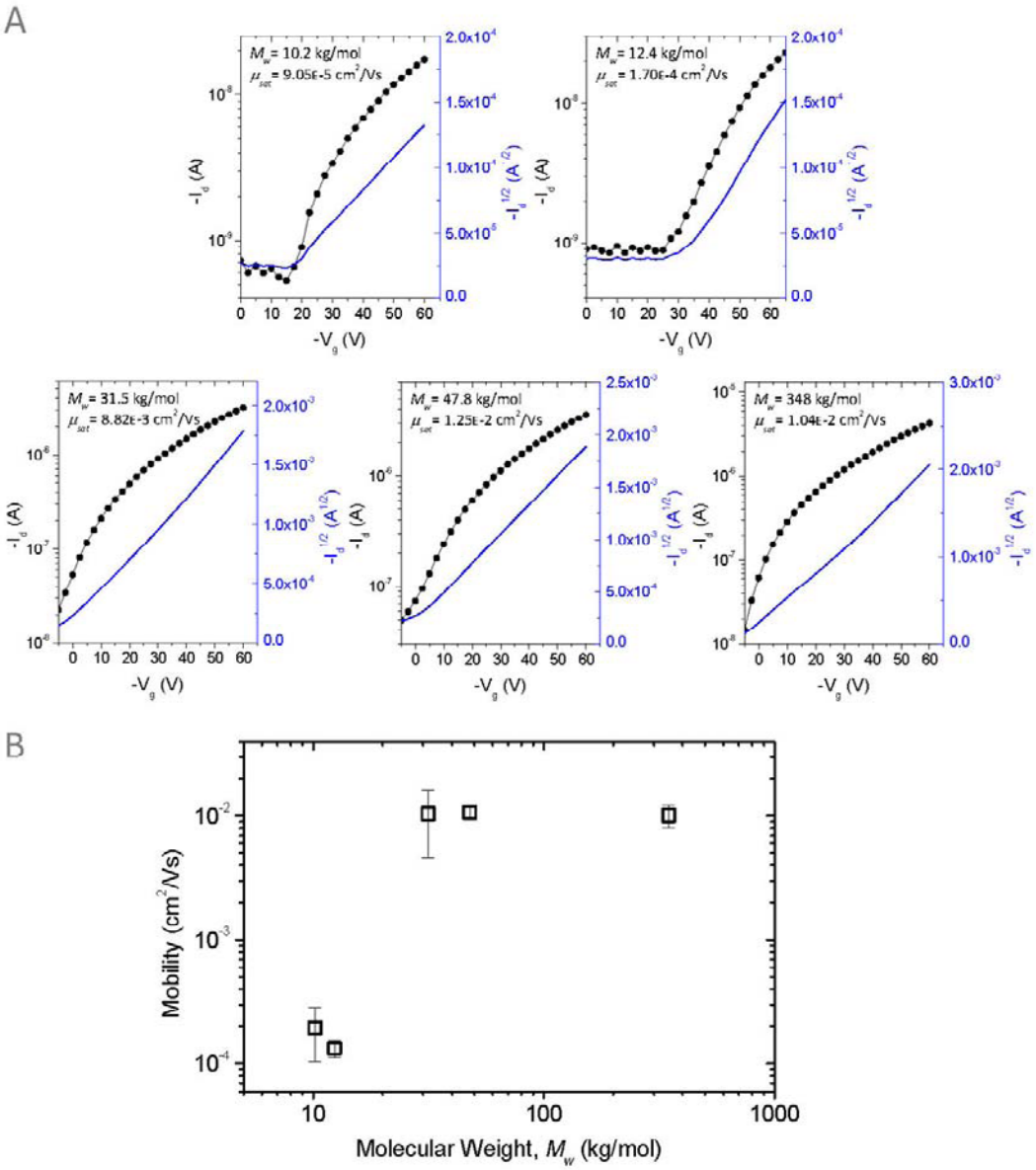


**Figure S9.** Electrical characterization of P3HT molecular weight series. (A) Representative transfer curves for P3HT transistors of varying molecular weight. In these cases, the devices were measured in saturation ($V_d$=-60V). (B) Average mobility as a function of P3HT molecular weight for devices tested in this work.

DOI: 10.1038/NMAT3722

## X. References


1 Clark, J., Chang, J.-F., Spano, F.C., Friend, R.H., & Silva, C., Determining exciton bandwidth and film microstructure in polythiophene films using linear absorption spectroscopy. *Applied Physics Letters* **94**, 163306-163303 (2009).

2 Clark, J., Silva, C., Friend, R.H., & Spano, F.C., Role of Intermolecular Coupling in the Photophysics of Disordered Organic Semiconductors: Aggregate Emission in Regioregular Polythiophene. *Physical Review Letters* **98**, 206406 (2007).

3 Spano, F.C., Modeling disorder in polymer aggregates: The optical spectroscopy of regioregular poly(3-hexylthiophene) thin films. *The Journal of Chemical Physics* **122**, 234701-234715 (2005).

4 Spano, F.C., Clark, J., Silva, C., & Friend, R.H., Determining exciton coherence from the photoluminescence spectral line shape in poly(3-hexylthiophene) thin films. *The Journal of Chemical Physics* **130**, 074904-074916 (2009).

5 Goris, L. *et al.*, Absorption phenomena in organic thin films for solar cell applications investigated by photothermal deflection spectroscopy. *Journal of Materials Science* **40**, 1413-1418 (2005).

6 Street, R.A., Northrup, J.E., & Salleo, A., Transport in polycrystalline polymer thin-film transistors. *Physical Review B* **71**, 165202 (2005).

7 Ko, S. *et al.*, Controlled Conjugated Backbone Twisting for an Increased Open-Circuit Voltage while Having a High Short-Circuit Current in Poly(hexylthiophene) Derivatives. *Journal of the American Chemical Society* **134**, 5222-5232 (2012).

8 Turner, S.T. *et al.*, Quantitative Analysis of Bulk Heterojunction Films Using Linear Absorption Spectroscopy and Solar Cell Performance. *Advanced Functional Materials* **21**, 4640-4652 (2011).

9 Cesar, B., Rawiso, M., Mathis, A., & Francois, B., Synthesis of polystyrene-poly-3 hexylthiophene block copolymers and characterization by X-rays and neutron scattering. *Synthetic Metals* **84**, 241-242 (1997).

10 Heffner, G.W. & Pearson, D.S., Molecular characterization of poly(3-hexylthiophene). *Macromolecules* **24**, 6295-6299 (1991).

11 McCulloch, B. *et al.*, Polymer Chain Shape of Poly(3-alkylthiophenes) in Solution Using Small-Angle Neutron Scattering. *Macromolecules* **46**, 1899-1907 (2013).

12 Data courtesy of J. E. Northrup, from: Northrup, J.E. Atomic and electronic structure of polymer organic semiconductors: P3HT, PQT, and PBTTT. *Physical Review B* **76**, 245202 (2007)

13 Malik, S. & Nandi, A.K., Crystallization mechanism of regioregular poly(3-alkyl thiophene)s. *Journal of Polymer Science Part B: Polymer Physics* **40**, 2073-2085 (2002).

14 Yi, Y.-B. & Sastry, A.M., Analytical approximation of the percolation threshold for overlapping ellipsoids of revolution. *Proceedings of the Royal Society of London A* **460**, 2353-2380 (2004).

15 Crist, B. & Cohen, J.B., Fourier analysis of polymer X-ray diffraction patterns. *Journal of Polymer Science: Polymer Physics Edition* **17**, 1001-1010 (1979).

16 Prosa, T.J., Moulton, J., Heeger, A.J., & Winokur, M.J., Diffraction Line-Shape Analysis of Poly(3-dodecylthiophene): A Study of Layer Disorder through the Liquid Crystalline Polymer Transition. *Macromolecules* **32**, 4000-4009 (1999).

17 Warren, B.E. & Averbach, B.L., The Separation of Cold-Work Distortion and Particle Size Broadening in X-Ray Patterns. *Journal of Applied Physics* **23**, 497-497 (1952).

18 Rivnay, J., Noriega, R., Kline, R.J., Salleo, A., & Toney, M.F., Quantitative analysis of lattice disorder and crystallite size in organic semiconductor thin films. *Physical Review B* **84**, 045203 (2011).

19 Hindeleh, A.M. & Hosemann, R., Paracrystals representing the physical state of matter. *Journal of Physics C: Solid State Physics* **21**, 4155-4170 (1988).

20 Hindeleh, A.M. & Hosemann, R., Microparacrystals: The intermediate stage between crystalline and amorphous. *Journal of Materials Science* **26**, 5127-5133 (1991).

21 Chabinyc, M.L., Toney, M.F., Kline, R.J., McCulloch, I., & Heeney, M., X-ray Scattering Study of Thin Films of Poly(2,5-bis(3-alkylthiophen-2-yl)thieno[3,2-b]thiophene). *Journal of the American Chemical Society* **129**, 3226-3237 (2007).

22 DeLongchamp, D.M. *et al.*, High Carrier Mobility Polythiophene Thin Films: Structure Determination by Experiment and Theory. *Advanced Materials* **19**, 833-837 (2007).

23 Wang, C.C. *et al.*, Microstructural Origin of High Mobility in High-Performance Poly(thieno-thiophene) Thin-Film Transistors. *Advanced Materials* **22**, 697-701 (2010).

24 Zhang, X. *et al.*, In-Plane Liquid Crystalline Texture of High-Performance Thienothiophene Copolymer Thin Films. *Advanced Functional Materials* **20**, 4098-4106 (2010).

25 Himmelberger, S. *et al.*, Effects of Confinement on Microstructure and Charge Transport in High Performance Semicrystalline Polymer Semiconductors. *Advanced Functional Materials* **23**, 2091-2098 (2013).

26 Jimison, L.H. *et al.*, Vertical confinement and interface effects on the microstructure and charge transport of P3HT thin films. *Journal of Polymer Science Part B: Polymer Physics* **51**, 611-620 (2013).